How Hemispherical Soft Fingertips Enhance Dexterity in Grasping and Manipulation

Takaniro Inoue *and* Shinichi Hirai
Dept. Robotics, Ritsumeikan University
Kusatsu, Shiga 525-8577, Japan
http://www.ritsumei.ac.jp/se/~hirai/

***Abstract*— We observed how a pair of 1-DOF fingers, whose fingertips are similar to humans in that they have a soft and hemispherical pad with a buttressing hard back plate, grasped and manipulated a rigid object. Based on the observations, we propose and validated a parallel distributed model that takes into account tangential deformation of the fingertips. We conclude that the number of degrees of freedom that the fingertips require to grasp and manipulate rigid objects is one less than the theoretical number required by rigid fingertips, and that the control law for the soft fingertips is simpler.**

I. Introduction

It is well known that we can grasp and manipulate objects with outstanding dexterity thanks to our highly developed brain, binocular brain, and abundance of motor and sensory nerves in our hands and fingers. It is also well known that, not only the anatomy of our hands, but also that of our fingers are well designed for grasping and manipulating objects. In addition to allowing us to pick up small objects, the fingernails are essential for the high level sensitivity and as a buttress for the pad. Because our fingers are so good at grasping and manipulating, much research in the field of robotics has focused on soft-fingered grasping and manipulation. However, little research has considered the shape and function of our fingernails.

Here, we examine the mechanics in grasping and manipulation by a simple robotic hand consisting of a pair of 1-DOF rotational fingers with hemispherical fingertips that have a soft pad and a hard back plate, similar to human fingers. We observe it grasping and manipulating an object, and show experimentally and theoretically that such fingers require fewer DOFs than corresponding fingers with hard fingertips. With the reduction in DOF, the control law is simpler, and fast sensing and visual monitoring of the object are not required.

Related work

Finite element (FE) analysis is often used when studying the deformation of objects, and can be used to describe deformation of a hemispherical soft fingertip exactly [1], [2], [3]. However, though FE analysis can be used to simulate grasping and manipulation numerically but cannot be applied to theoretical analysis of grasping and manipulation due to its complex formulation. In other words, FE analysis yields a *procedural* deformation model, which allows us to simulate the deformation of objects but cannot be applied to theoretical analysis. According to the principle of Occam's razor, we should choose a simple model to analyze and explain grasping and manipulation by soft fingertips.

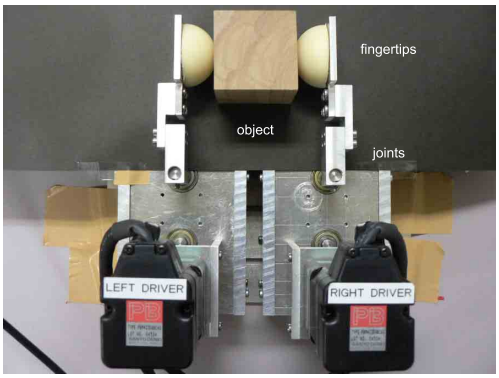

Fig. 1. A pair of 1-DOF fingers with soft fingertips

The Hertzian contact model provides a simple closed-form description of the contact between two quadratic surfaces of elastic objects [4], but because the surfaces are assumed to be open-ended, it cannot be applied to a hemispherical elastic fingertip with a rigid back plate. Arimoto *et al.* formulated dynamics of pinching by a pair of soft fingertips [5], and used a radially distributed deformation model to analyze the mechanics of a soft fingertip [6]. Based on the concept of *stability on a manifold*, they showed theoretically that a 2-DOF finger and a 1-DOF finger can together realize secure grasping and posture control [7], [8]. Moreover, Arimoto and Doulgeri formulated *rolling contact* between a grasped object and fingers with rigid tips and also showed that a 2-DOF finger and a 1-DOF finger can together realize secure grasping and posture control. This implies that rolling contact between an object and fingertips is the key to stable grasping and posture control, and that a third DOF is necessary to balance the moments acting on a grasped object. However, from our observations below, in addition to being able to grasp a rigid object, a pair of 1-DOF fingers with soft hemispherical fingertips can control the orientation of the object, which calls for a new model.

II. Observation of Soft-fingered Grasping and Manipulation

A. Object pinching by a pair of 1-DOF fingers

Let us observe the grasping and manipulation of a rigid object by a pair of soft-fingertipped finger each with

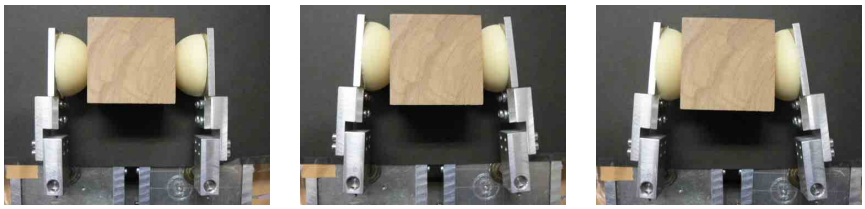

(a) (b) (c)

Fig. 2. Deformation of fingertips when two fingers rotate in opposite directions

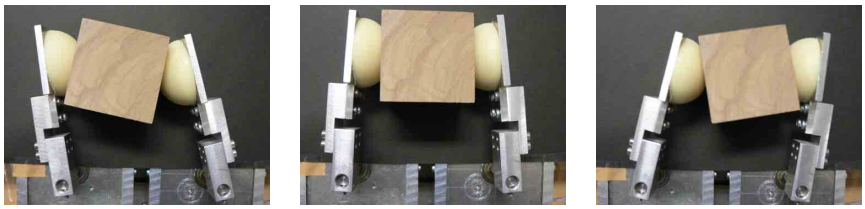

(a) (b) (c)

Fig. 3. Motion of object when two fingers rotate in the same direction

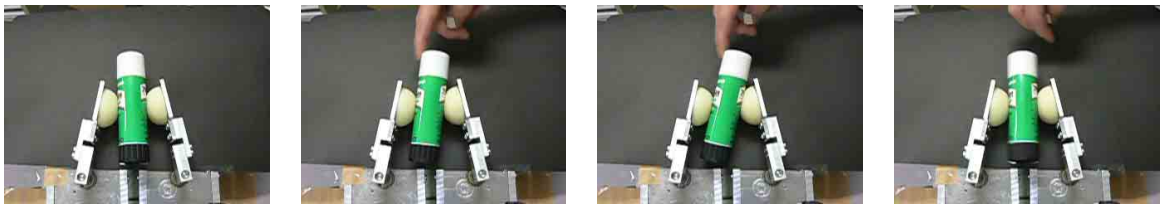

(a) (b) (c) (d)

Fig. 4. Rotation of pinched object by external force

a 1-DOF rotational joint driven by an actuator. Figure 1 shows such a pair of fingers, driven by DC motors, grasping a rectangular rigid object. When the two fingertips move inward, that is, toward each other, they become more deformed, suggesting that they are applying a larger grasping force, as shown in Figure 2. This observation suggests that the grasping force can be regulated by the two joint angles, *i.e.*, secure grasping can be achieved by a pair of 1-DOF fingers with soft fingertips. When one fingertip moves inward and the other outward, that is, both rotate in the same direction, the object rotates in the opposite direction, implying that the orientation of the object can be regulated by the two joint angles, as shown in Figure 3. This observation suggests that orientation can be controlled by a pair of 1-DOF fingers with soft fingertips.

The above observations suggest that a pair of 1-DOF fingers with soft fingertips can control both grasping force and object orientation independently, in contrast to a conclusion by Arimoto *et al.*, in their analysis of the dynamics of soft-fingered grasping and manipulation, that a pair of 1-DOF rotational fingers with soft fingertips can control grasping force but not object orientation. They asserted that both a 1-DOF finger and a 2-DOF finger are required to control both grasping force and object orientation. Thus, there is a discrepancy between our observations and their claim, so their model may not be valid in this case. In their *radially distributed* model, Figure 5-(a), the contact force passes through the center of a soft hemispherical fingertip, and its magnitude is dependent on the maximum displacement of the fingertip but not on the relative orientation between the fingertip and the object. Since two contact forces would apply a non-zero moment to the object, an additional DOF is needed to cancel out the moment and to stabilize object rotation. Therefore, we need another fingertip model that properly also describes the maximum displacement and the relative orientation between the fingertip and the object.

B. Rotation of pinched object by external force

When an external force is applied to the rigid object pinched by the two fingers fixed at given orientations, the fingertips deform the object may rotate, as shown in Figure 4. When the applied force is relaxed, the object returns to its initial orientation. The object, therefore, does not slip, and so there are geometric constraints, which are referred to as *rolling constraints*. On giving constant values to both of the joint angles and solving the two rolling constraints, we find that the orientation of the grasped object is constant. This is another discrepancy with the claim by Arimoto *et al*, and it is due to the lack of tangential deformation in their model. In their radially distributed model, any point on the hemispherical surface of a soft fingertip moves along a line normal to the surface, which determines the shrinkage of an elastic element inside the fingertip. That is, each elastic element deforms normally but not tangentially. Therefore, it is necessary to introduce tangential deformation into the fingertip model to describe the rotation of a pinched object

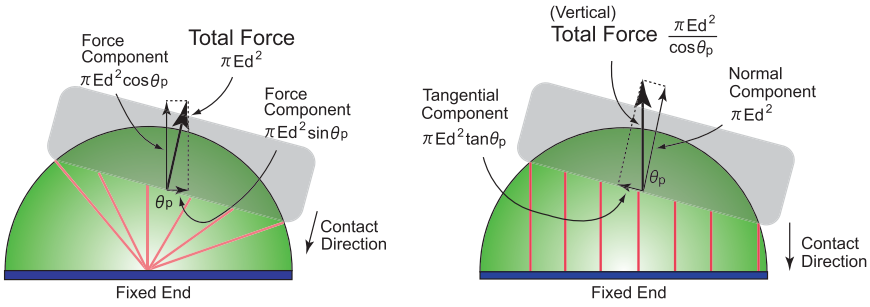

(a) radially distributed model (b) parallel distributed model

Fig. 5. Fingertip models

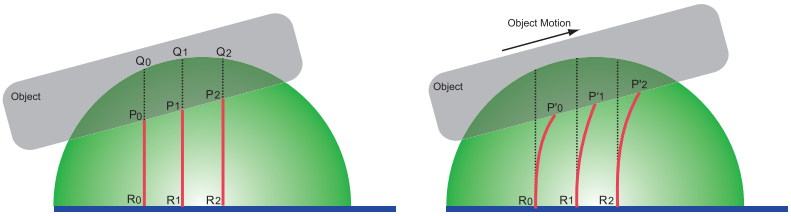

(a) without tangential deformation (b) with tangential deformation

Fig. 6. Tangential deformation in the parallel distributed model

by an external force.

III. Soft Fingertip Models

Let us build a model based on the observations of soft fingertips described in Section II. Figure 5-(a) shows the radially distributed model, which has been applied previously to the analysis of soft-fingered grasping and manipulation [5], [6]. Let a be the radius of a hemispherical fingertip in its natural shape and E be Young's modulus of the material of the fingertip. Elastic elements are distributed radially inside the fingertip. As all of the elements have the same natural length, which is given by the radius a of the fingertip, they all have the same spring constant $E\,\mathrm{d}S/a$, where $\mathrm{d}S$ denotes the element's cross-sectional area. When the soft fingertips contact the planar surface of the rigid object, they deform, thereby applying elastic forces. Let d be the maximum displacement of the soft fingertip and θ_p be the relative orientation between the fingertip and the object. Each elastic element generates an elastic force according to how much it is deformed. Integrating all elastic forces gives the resultant contact force:

$$F_\mathrm{radial} = \pi E d^2. \tag{1}$$

The force passes through the center of the fingertip, as illustrated in the figure. Note that the magnitude of the force depends on the maximum displacement d but is independent of the relative orientation θ_p.

Figure 5-(b) shows our proposed parallel distributed model. We summarize the derivation of the model. See [9] in detail. The elastic elements are distributed in parallel inside the soft fingertip. Note that the natural length of each element is dependent on the element's position. Let (x, y) be the position of an elastic element. Then, its natural length is given by $(a^2 - x^2 - y^2)^{1/2}$ and the spring constant of the element is given by

$$\frac{E\,\mathrm{d}S}{\sqrt{a^2 - (x^2 + y^2)}}.$$

Each elastic element generates an elastic force according to its shrinkage. Integrating all elastic forces gives the resultant contact force. Displacement d and angle θ_p determine the shrinkage of each elastic element. Computing the integral yields the magnitude of the contact force given by

$$F_\mathrm{perp} = \frac{\pi E d^2}{\cos\theta_\mathrm{p}}. \tag{2}$$

The force is perpendicular to the planar surface behind the fingertip, as illustrated in the figure. Note that the force magnitude depends on both the maximum displacement d and the relative orientation θ_p. This dependency is due to the hemispherical shape of the soft fingertip subtended by a fixed rigid end, which is similar to a human finger consisting of a soft fingertip and a hard fingernail. The parallel distributed model reflects this structure consisting of a soft fingertip and a hard fingernail. Integrating potential energies caused by the perpendicular deformation of individual elastic elements in the parallel distributed model yields the potential energy of the fingertip as follows:

$$U_\mathrm{perp}(d, \theta_\mathrm{p}) = \frac{\pi E d^3}{3\cos^2\theta_\mathrm{p}}. \tag{3}$$

Note that the potential energy depends not only on the maximum displacement d but also on the relative orientation θ_p.

As described in Section II, tangential deformation should be introduced into the parallel distributed model so that a pinched object can rotate when an external force is

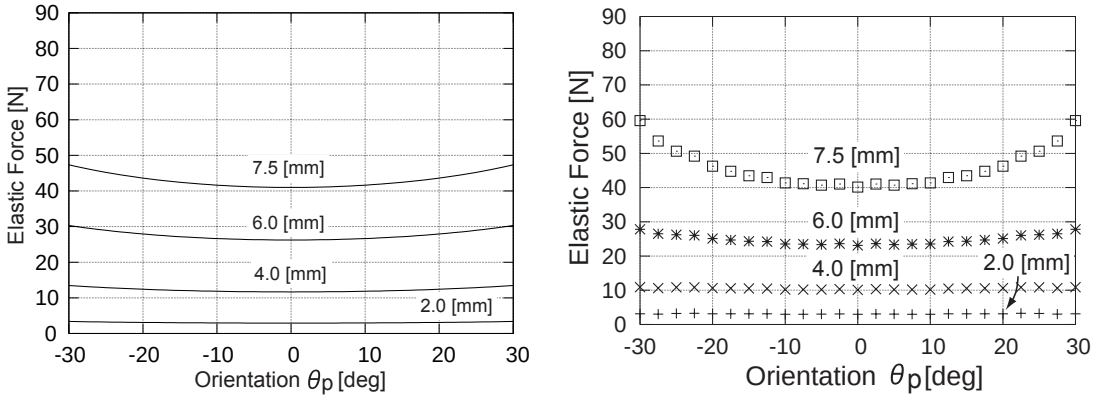

(a) simulation (b) experiment

Fig. 7. Simulation and experimental results

applied. Figure 6 shows the tangential deformation model. Assume that the fingertip does not deform tangentially when in contact with the rigid object, as illustrated in Figure 6-(a). In the parallel distributed model, point Q_k on the fingertip surface moves to P_k, shrinking the elastic element of natural length $\mathrm{Q}_k\mathrm{R}_k$ to $\mathrm{P}_k\mathrm{R}_k$. Assuming that the rigid object moves tangentially by displacement d_t as shown in Figure 6-(b), the point P_k moves to P'_k, and $\mathrm{P}_k\mathrm{P}'_k$ determines the tangential deformation of the elastic element. Given the position and the orientation of an object, we can calculate the perpendicular deformation $\mathrm{Q}_k\mathrm{P}_k$ and tangential deformation $\mathrm{P}_k\mathrm{P}'_k$ of each elastic element. The tangential deformation determines the tangential force generated by the element. For the sake of simplicity, we assume that Young's modulus E characterizes the linear relationship between the tangential force and the tangential deformation. Integrating tangential forces for all elastic elements gives the resultant tangential force:

$$F_{\mathrm{tangent}} = 2\pi E d d_\mathrm{t}. \tag{4}$$

We should emphasize that perpendicular and lateral components of the contact force in the radially distributed model are given by $F_{\mathrm{radial}} \cos\theta_\mathrm{p}$ and $F_{\mathrm{radial}} \sin\theta_\mathrm{p}$, respectively, compared with $F_{\mathrm{perp}} + F_{\mathrm{tangent}} \sin\theta_\mathrm{p}$ and $F_{\mathrm{tangent}} \cos\theta_\mathrm{p}$ in the parallel distributed model. Integrating potential energies caused by tangential deformation of individual elastic elements in the parallel distributed model yields the total potential energy caused by tangential deformation as follows:

$$U_{\mathrm{tangent}}(d, d_\mathrm{t}, \theta_\mathrm{p}) = \pi E\{d^2 d_\mathrm{t} \tan\theta_\mathrm{p} + d d_\mathrm{t}^2\}. \tag{5}$$

As the perpendicular and tangential displacements are not orthogonal, the above equation shows the coupling between them. Consequently, the total potential energy of a hemispherical soft fingertip in the parallel distributed model can be formulated as follows:

$$\begin{aligned} U_{\mathrm{parallel}}(d, d_\mathrm{t}, \theta_\mathrm{p}) &= U_{\mathrm{perp}}(d, \theta_\mathrm{p}) + \\ & \quad U_{\mathrm{tangent}}(d, d_\mathrm{t}, \theta_\mathrm{p}). \end{aligned} \tag{6}$$

Note that this potential energy is dependent on the maximum displacement d, tangential displacement d_t, and relative angle θ_p.

IV. Experimental Verification of Fingertip Models

We experimentally verified the parallel distributed model proposed in Section III. We made a hemispherical silicon rubber fingertip with a diameter of 40 mm. From a tension and compression test, Young's modulus of the silicon rubber was $E = 0.232$ MPa. We obtained the resultant perpendicular force applied by the fingertip by summing the pressure measured by an array of pressure sensors on the back of the fingertip. Figure 7 compares the results of our simulation and experiment. The horizontal and vertical axes in the graphs denote the relative angle between the fingertip and an object and the magnitude of the elastic force, respectively. The maximum displacements are 2.0 mm, 4.0 mm, 6.0 mm, and 7.5 mm. As shown in Figure 7-(a), the magnitude of the contacting force is minimum at $\theta_\mathrm{p} = 0$ as long as the maximum displacement d remains constant. The experimental results shown in Figure 7-(b) also show that the magnitude is minimum at $\theta_\mathrm{p} = 0$. Consequently, the force model in the parallel distributed model agrees with the experimental results. Note that in the radially distributed model, the magnitude of the force remains constant and the component perpendicular to the back plate is maximum rather than minimum at $\theta_\mathrm{p} = 0$. Hence, the radially distributed model does not agree with the experimental results.

V. Dynamics of Soft-fingered Grasping and Manipulation

Let us apply the parallel distributed model to the pair of 1-DOF fingers with soft hemispherical fingertips grasping and manipulating the rigid object in Figure 8. The right finger rotates around point S and the left finger rotates around point T, and θ_1 and θ_2 are the rotational angles of the right and left fingers which have the same dimensions. Let L be the length between the center of the hemispherical fingertip and the finger rotational joint, W_fi be the distance between the two rotational joints, and d_fi be the thickness

of fingers. Let O_1 be the center of the right fingertip and (O_{1x}, O_{1y}) be its position, which is given by

$$O_{1x} = W_{\rm fi} - L\sin\theta_1 - d_{\rm fi}\cos\theta_1,$$
$$O_{1y} = L\cos\theta_1 - d_{\rm fi}\sin\theta_1.$$

Let O_2 be the center of the left fingertip and (O_{2x}, O_{2y}) be its position, which is given by

$$O_{2x} = -W_{\rm fi} + L\sin\theta_1 + d_{\rm fi}\cos\theta_1,$$
$$O_{2y} = L\cos\theta_1 - d_{\rm fi}\sin\theta_1.$$

The width of the body of width is $W_{\rm obj}$. Let $(x_{\rm obj}, y_{\rm obj})$ be the positional vector and $\theta_{\rm obj}$ be the orientation angle of the object. The relative angle between the object and the right finger is $\theta_1 - \theta_{\rm obj}$, while the angle between the object and the left finger is $\theta_2 + \theta_{\rm obj}$.

Let $d_{\rm n1}$ and $d_{\rm t1}$ be the maximum and and tangential displacements of the right fingertip. Let us formulate geometric constraints imposed by the contact between the object and the right fingertip. These constraints depend on the maximum normal and tangential displacements $d_{\rm n1}$ and $d_{\rm t1}$, angle θ_1, the object position $(x_{\rm obj}, y_{\rm obj})$, and the object orientation $\theta_{\rm obj}$. Computing the projection of vector $G\vec{O}_1$ along the maximum deformation, we have the following geometric constraint:

$$C_1^{\rm H} \triangleq -(x_{\rm obj} - O_{1x})C_{\rm obj} - (y_{\rm obj} - O_{1y})S_{\rm obj} - (a - d_{\rm n1}) + \frac{W_{\rm obj}}{2} = 0, \qquad (7)$$

where $C_{\rm obj} = \cos\theta_{\rm obj}$ and $S_{\rm obj} = \sin\theta_{\rm obj}$ are abbreviations. The above equation provides a holonomic constraint. Assume that no slip happens between the object and fingertip. Note that the projection of vector $G\vec{O}_1$ along the tangential deformation is given by $GQ_1 = -(x_{\rm obj} - O_{1x})\sin\theta_{\rm obj} + (y_{\rm obj} - O_{1y})\cos\theta_{\rm obj}$. Since the tangential velocity of the fingertip coincides with the tangential velocity of the object at the contacting point, we have the following equation:

$$C_1^{\rm N} \triangleq \dot{GQ}_1 + a(\dot\theta_1 - \dot\theta_{\rm obj}) + \dot d_{\rm 1t} = 0. \qquad (8)$$

This equation provides a nonholonomic constraint. Let $d_{\rm n2}$ and $d_{\rm t2}$ be the maximum and tangential displacements of the left fingertip. We can also formulate two geometric constraints caused by the contact between the object and the left fingertip: one holonomic constraint

$$C_2^{\rm H} \triangleq (x_{\rm obj} - O_{2x})C_{\rm obj} + (y_{\rm obj} - O_{2y})S_{\rm obj} - (a - d_{\rm n2}) + \frac{W_{\rm obj}}{2} = 0 \qquad (9)$$

and one nonholonomic constraint

$$C_2^{\rm N} \triangleq \dot{GQ}_2 + a(\dot\theta_2 + \dot\theta_{\rm obj}) + \dot d_{\rm 2t} = 0, \qquad (10)$$

where $GQ_2 = -(x_{\rm obj} - O_{2x})\sin\theta_{\rm obj} + (y_{\rm obj} - O_{2y})\cos\theta_{\rm obj}$ denotes the projection of vector $G\vec{O}_2$ along the tangential deformation.

The process of grasping and manipulation by a pair of 1-DOF rotational fingers with soft fingertips can be described

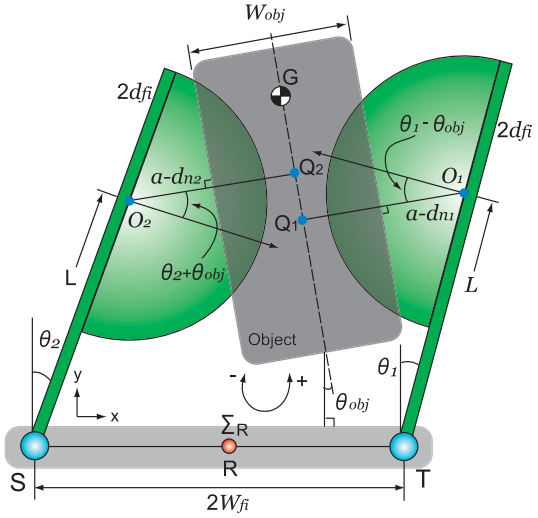

Fig. 8. Simulation model

by a set of nine generalized coordinates: object coordinates $x_{\rm obj}$ and $y_{\rm obj}$, object orientation $\theta_{\rm obj}$, and for the two fingers respectively, rotational angles θ_1 and θ_2, maximum normal deformations $d_{\rm n1}$ and $d_{\rm n2}$, and tangential deformations $d_{\rm t1}$ and $d_{\rm t2}$. Recall that two holonomic constraints (7) and (9) and two nonholonomic constraints (8) and (10) are imposed during the process.

Let $m_{\rm obj}$ be the mass of the object and $I_{\rm obj}$ be the moment of inertia of the object around its center of gravity. Assume that the weight of the two fingers are negligible. Assume that the object and the two fingers move in a vertical plane, where gravitational forces act along the y-axis in its negative direction. The potential energy of the system is then given by the sum of the elastic potential energies of the two fingertips and the gravitational energy of the object as follows:

$$\begin{aligned} U &= U_{\rm parallel}(d_{\rm n1}, d_{\rm t1}, \theta_1 - \theta_{\rm obj}) + \\ &\quad U_{\rm parallel}(d_{\rm n2}, d_{\rm t2}, \theta_2 + \theta_{\rm obj}) + \\ &\quad m_{\rm obj} g\, y_{\rm obj}, \end{aligned} \qquad (11)$$

Let $I_{\rm finger}$ be the moment of inertia of each finger around its rotational axis. Assuming that mass transfer due to the deformation of each fingertip is negligible, the kinetic energy of the system can be formulated as follows:

$$\begin{aligned} T &= \frac{1}{2}m_{\rm obj}(\dot x_{\rm obj}^2 + \dot y_{\rm obj}^2) + \frac{1}{2}I_{\rm obj}\dot\theta_{\rm obj}^2 + \\ &\quad \frac{1}{2}I_{\rm finger}\dot\theta_1^2 + \frac{1}{2}I_{\rm finger}\dot\theta_2^2. \end{aligned} \qquad (12)$$

From eqs.(11) and (12), we can formulate the Lagrange equations of motion of a pair of fingers pinching a rigid object. Lagrangean with holonomic constraints is described by

$$\mathcal{L} = T - U + \lambda_1^{\rm H} C_1^{\rm H} + \lambda_2^{\rm H} C_2^{\rm H}, \qquad (13)$$

where $\lambda_1^{\rm H}$ and $\lambda_2^{\rm H}$ denote Lagrange multipliers corresponding to the two holonomic constraints. Incorporating nonholonomic constraints, we have nine Lagrange equations of

motion corresponding to the nine generalized coordinates:

$$\begin{aligned}
\frac{\mathrm{d}}{\mathrm{d}t}\frac{\partial \mathcal{L}}{\partial \dot{x}_{\mathrm{obj}}} - \frac{\partial \mathcal{L}}{\partial x_{\mathrm{obj}}} &= \frac{\partial}{\partial \dot{x}_{\mathrm{obj}}}\{\lambda_1^{\mathrm{N}} C_1^{\mathrm{N}} + \lambda_2^{\mathrm{N}} C_2^{\mathrm{N}}\},\\
\frac{\mathrm{d}}{\mathrm{d}t}\frac{\partial \mathcal{L}}{\partial \dot{y}_{\mathrm{obj}}} - \frac{\partial \mathcal{L}}{\partial y_{\mathrm{obj}}} &= \frac{\partial}{\partial \dot{y}_{\mathrm{obj}}}\{\lambda_1^{\mathrm{N}} C_1^{\mathrm{N}} + \lambda_2^{\mathrm{N}} C_2^{\mathrm{N}}\},\\
\frac{\mathrm{d}}{\mathrm{d}t}\frac{\partial \mathcal{L}}{\partial \dot{\theta}_{\mathrm{obj}}} - \frac{\partial \mathcal{L}}{\partial \theta_{\mathrm{obj}}} &= \frac{\partial}{\partial \dot{\theta}_{\mathrm{obj}}}\{\lambda_1^{\mathrm{N}} C_1^{\mathrm{N}} + \lambda_2^{\mathrm{N}} C_2^{\mathrm{N}}\},\\
\frac{\mathrm{d}}{\mathrm{d}t}\frac{\partial \mathcal{L}}{\partial \dot{\theta}_1} - \frac{\partial \mathcal{L}}{\partial \theta_1} &= \frac{\partial}{\partial \dot{\theta}_1}\{\lambda_1^{\mathrm{N}} C_1^{\mathrm{N}} + \lambda_2^{\mathrm{N}} C_2^{\mathrm{N}}\},\\
\frac{\mathrm{d}}{\mathrm{d}t}\frac{\partial \mathcal{L}}{\partial \dot{\theta}_2} - \frac{\partial \mathcal{L}}{\partial \theta_2} &= \frac{\partial}{\partial \dot{\theta}_2}\{\lambda_1^{\mathrm{N}} C_1^{\mathrm{N}} + \lambda_2^{\mathrm{N}} C_2^{\mathrm{N}}\},\\
\frac{\mathrm{d}}{\mathrm{d}t}\frac{\partial \mathcal{L}}{\partial \dot{d}_1} - \frac{\partial \mathcal{L}}{\partial d_{\mathrm{n}1}} &= \frac{\partial}{\partial \dot{d}_1}\{\lambda_1^{\mathrm{N}} C_1^{\mathrm{N}} + \lambda_2^{\mathrm{N}} C_2^{\mathrm{N}}\},\\
\frac{\mathrm{d}}{\mathrm{d}t}\frac{\partial \mathcal{L}}{\partial \dot{d}_2} - \frac{\partial \mathcal{L}}{\partial d_{\mathrm{n}2}} &= \frac{\partial}{\partial \dot{d}_2}\{\lambda_1^{\mathrm{N}} C_1^{\mathrm{N}} + \lambda_2^{\mathrm{N}} C_2^{\mathrm{N}}\},\\
\frac{\mathrm{d}}{\mathrm{d}t}\frac{\partial \mathcal{L}}{\partial \dot{d}_{1\mathrm{t}}} - \frac{\partial \mathcal{L}}{\partial d_{\mathrm{t}1}} &= \frac{\partial}{\partial \dot{d}_{1\mathrm{t}}}\{\lambda_1^{\mathrm{N}} C_1^{\mathrm{N}} + \lambda_2^{\mathrm{N}} C_2^{\mathrm{N}}\},\\
\frac{\mathrm{d}}{\mathrm{d}t}\frac{\partial \mathcal{L}}{\partial \dot{d}_{2\mathrm{t}}} - \frac{\partial \mathcal{L}}{\partial d_{\mathrm{t}2}} &= \frac{\partial}{\partial \dot{d}_{2\mathrm{t}}}\{\lambda_1^{\mathrm{N}} C_1^{\mathrm{N}} + \lambda_2^{\mathrm{N}} C_2^{\mathrm{N}}\},
\end{aligned} \tag{14}$$

where λ_1^{N} and λ_2^{N} denote Lagrange multipliers corresponding to the two nonholonomic constraints. Let c_{n} and c_{t} be viscous moduli of a fingertip along the normal and tangential directions. Then, we can formulate viscous terms, which are incorporated into the above Lagrange equations of motion.

Consequently, dynamics of grasping and manipulation of an object by a pair of 1-DOF fingers with soft fingertips is formulated by a set of Lagrange equations of motion (14) with four constraints (7), (8), (9), and (10).

VI. Simulation of Soft-fingered Grasping and Manipulation

A. Numerical integration of Lagrange equations of motion under geometric constraints

We can simulate the dynamic process of grasping and manipulation by a pair of fingers with soft fingertips by solving a set of Lagrange equations of motions (14) under geometric constraints (7), (8), (9), and (10). Let us convert the geometric constraints into differential equations to incorporate them into the Lagrange equations of motion through the constraint stabilization method [10]. The constraint stabilization method converts the two holonomic constraints (7) and (9) into the following differential equations:

$$\begin{aligned}
\ddot{C}_1^{\mathrm{H}} + 2\alpha \dot{C}_1^{\mathrm{H}} + \alpha^2 C_1^{\mathrm{H}} = 0,\\
\ddot{C}_2^{\mathrm{H}} + 2\alpha \dot{C}_2^{\mathrm{H}} + \alpha^2 C_2^{\mathrm{H}} = 0,
\end{aligned} \tag{15}$$

where parameter α is a sufficiently large constant. Note that the above equations describe critical damping, implying that the value of each holonomic constraint converges to zero even if the constraint is broken due to numerical integration of the Lagrange equations of motion. The constraint stabilization method converts the two nonholonomic constraints (8) and (10) into the following differential equations:

$$\begin{aligned}
\alpha \dot{C}_1^{\mathrm{N}} + \beta C_1^{\mathrm{N}} = 0,\\
\alpha \dot{C}_2^{\mathrm{N}} + \beta C_2^{\mathrm{N}} = 0,
\end{aligned} \tag{16}$$

where parameter β is a sufficiently large constant. Note that the above equations describe exponential damping, implying that the value of each nonholonomic constraint also converges to zero even if the constraint is broken due to numerical integration of the Lagrange equations of motion.

A set of Lagrange equations of motion (14) and differential equations to stabilize geometric constraints (15) and (16) involve nine generalized coordinates and four multipliers, which are unknown variables. Thus, numerically solving thirteen differential equations (14), (15), and (16) yields nine generalized coordinates and four multipliers. Let us introduce a collective vector consisting of generalized coordinates $\boldsymbol{q} = [x_{\mathrm{obj}}, y_{\mathrm{obj}}, \theta_{\mathrm{obj}}, \theta_1, \theta_2, d_{\mathrm{n}1}, d_{\mathrm{n}2}, d_{\mathrm{t}1}, d_{\mathrm{t}2}]^{\mathrm{T}}$ and a collective vector consisting of generalized velocities $\boldsymbol{p} = [\dot{x}_{\mathrm{obj}}, \dot{y}_{\mathrm{obj}}, \dot{\theta}_{\mathrm{obj}}, \dot{\theta}_1, \dot{\theta}_2, \dot{d}_1, \dot{d}_2, \dot{d}_{1\mathrm{t}}, \dot{d}_{2\mathrm{t}}]^{\mathrm{T}}$. Let $\boldsymbol{\lambda}_{\mathrm{H}} = [\lambda_1^{\mathrm{H}}, \lambda_2^{\mathrm{H}}]^{\mathrm{T}}$ be a vector consisting of Lagrange multipliers corresponding to holonomic constraints, and $\boldsymbol{\lambda}_{\mathrm{N}} = [\lambda_1^{\mathrm{N}}, \lambda_2^{\mathrm{N}}]^{\mathrm{T}}$ be a vector consisting of Lagrange multipliers corresponding to nonholonomic constraints. Let us substitute $\boldsymbol{p} = \dot{\boldsymbol{q}}$ into differential equations (14), (15), and (16) to collect terms with a set of time derivatives $\dot{\boldsymbol{p}}$ and Lagrange multipliers $\boldsymbol{\lambda}_{\mathrm{H}}$ and $\boldsymbol{\lambda}_{\mathrm{N}}$ into the left side. The definition of vector $\boldsymbol{p}$, a set of Lagrange equations of motion (14), differential equations to stabilize holonomic constraints (15), and differential equations to stabilize nonholonomic constraints (16) can be collectively described by

$$\begin{bmatrix} I & O & O & O \\ O & M & -\phi_{\mathrm{H}}^{\mathrm{T}} & -\phi_{\mathrm{N}}^{\mathrm{T}} \\ O & -\phi_{\mathrm{H}} & O & O \\ O & -\phi_{\mathrm{N}} & O & O \end{bmatrix} \begin{bmatrix} \dot{\boldsymbol{q}} \\ \dot{\boldsymbol{p}} \\ \boldsymbol{\lambda}_{\mathrm{H}} \\ \boldsymbol{\lambda}_{\mathrm{N}} \end{bmatrix} = \begin{bmatrix} \boldsymbol{p} \\ \boldsymbol{f} \\ \boldsymbol{C}_{\mathrm{H}} \\ \boldsymbol{C}_{\mathrm{N}} \end{bmatrix},$$

where I denotes the nine by nine identity matrix and O denotes the nine by nine zero matrix. Matrix M is a nine by nine inertia matrix, which depends on a set of generalized coordinates $\boldsymbol{q}$. Matrices ϕ_{H} and ϕ_{N} are nine by nine matrices, which depend on a set of generalized coordinates $\boldsymbol{q}$ and a set of generalized velocities $\boldsymbol{p}$. Vectors $\boldsymbol{f}$, $\boldsymbol{C}_{\mathrm{H}}$ and $\boldsymbol{C}_{\mathrm{N}}$ are nine dimensional vectors, which depend on a set of generalized coordinates $\boldsymbol{q}$ and a set of generalized velocities $\boldsymbol{p}$. The coefficient matrix on the left side of the above equation is regular, so $\dot{\boldsymbol{q}}$, $\dot{\boldsymbol{p}}$, $\boldsymbol{\lambda}_{\mathrm{H}}$, and $\boldsymbol{\lambda}_{\mathrm{N}}$ can be solved in the above linear equation. We can obtain $\boldsymbol{q}$ and $\boldsymbol{p}$ by applying a numerical integration of differential equations to this computation process.

B. Simulation results

Figure 9 shows a simulation, based on the parallel distributed model, of a pair of the 1-DOF fingers controlling the orientation of an object. We used the parameters listed in Table I. Figure 9-(a) shows the initial contact position between the fingers and the object, in which the fingertip

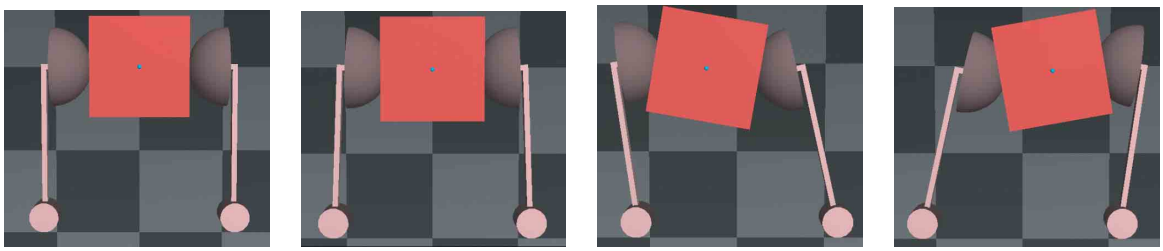

(a) (b) (c) (c)

Fig. 9. Simulation of fingertips controlling orientation of an object

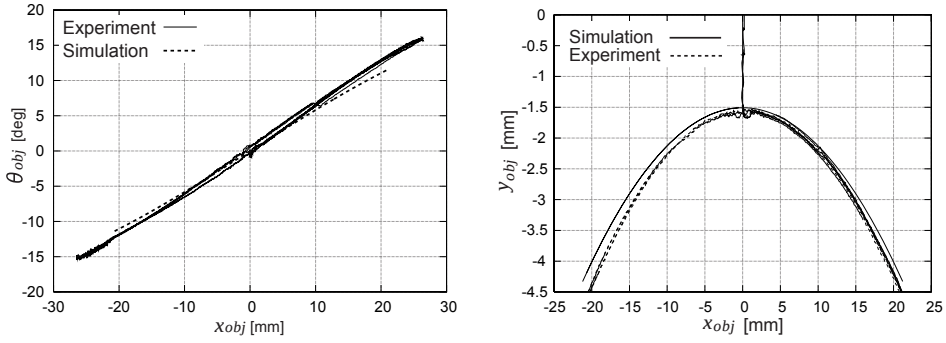

(a) orientation (b) position

Fig. 10. Comparison of simulation and experimental results

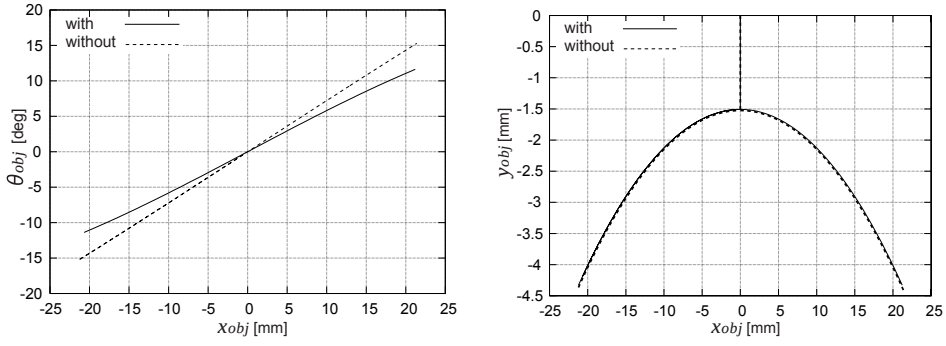

(a) orientation (b) position

Fig. 11. Comparison of simulation results with and without tangential deformation

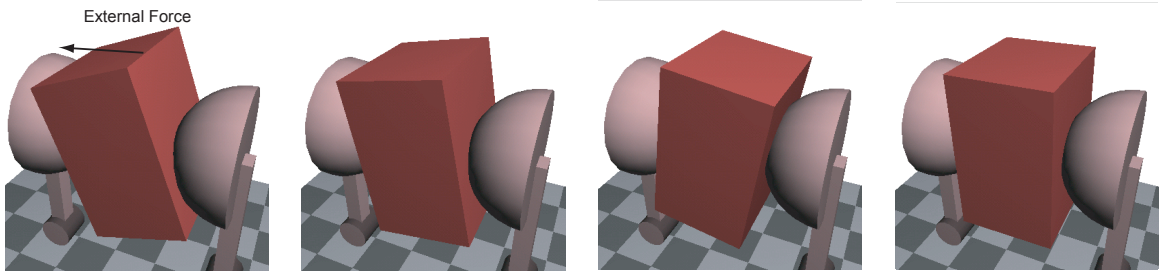

(a) (b) (c) (d)

Fig. 12. Simulation of orientation of pinched object by external force

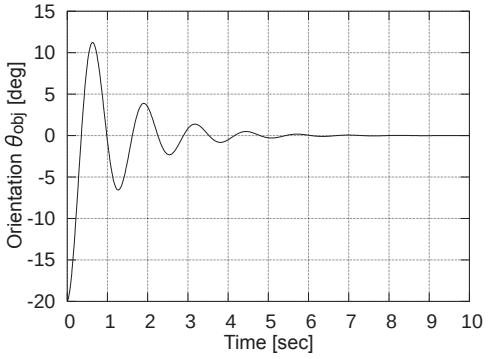

Fig. 13. Simulated object orientation angle

TABLE I

SIMULATION PARAMETERS

a	20 mm
E	0.232 MPa
$c_{\rm n}$	300 N/(m/s)
$c_{\rm t}$	300 N/(m/s)
L	76.2 mm
$d_{\rm fi}$	4 mm
$2W_{\rm fi}$	97 mm
$I_{\rm finger}$	125 kg·mm^2

$W_{\rm obj}$	49 mm
$m_{\rm obj}$	0.3 kg
$I_{\rm obj}$	125 kg·mm^2
α	20000
β	10000

was not deformed, and Figure 9-(b) shows the initial grasping position, in which both fingertips are deformed the same. In Figure 9-(c), the fingers have both rotated counterclockwise and the object has rotated clockwise, while in Figure 9-(d), the fingers have rotated clockwise and the object has rotated counterclockwise. The results of the simulation agree with the observations shown in Figure 3. The simulation suggests that a pair of 1-DOF rotational fingers with soft fingertips can control the orientation of a pinched object.

Figure 10 compares the simulation and experimental results of how the fingertips controlled the orientation of the pinched object. In Figure 10-(a), the way in which the object's orientation angle $\theta_{\rm obj}$ changes with its coordinate $x_{\rm obj}$ in the simulation was almost the same as how it changes in the experiment. Also, in Figure 10-(b), the relative changes in the object's coordinates $x_{\rm obj}$ and $y_{\rm obj}$ in the simulation were almost the same as those in the experiment.

Figure 11 compares simulations based on the parallel model with and without tangential deformation of the fingertips. In Figure 11-(a), the slope of the plot of the object's orientation angle $\theta_{\rm obj}$ against its coordinate $x_{\rm obj}$ is steeper without than with tangential deformation. Since the simulation results based on the parallel model with tangential deformation agree well with the experimental results, tangential deformation probably occurs in actual grasping and manipulation. In Figure 10-(b), the path of the pinched object is the same regardless of tangential deformation. Note that the center of the pinched object lies on a line between the two points of contact in the initial grasping position, as shown in Figure 9-(a), which may be

TABLE II

SEQUENCE OF MOTIONS

initial state	both fingers grasp an object in parallel
motion 1	$(\theta_1^{\rm d}, \theta_2^{\rm d}) = (6\,{\rm deg},\ 6\,{\rm deg})$
motion 2	$(\theta_1^{\rm d}, \theta_2^{\rm d}) = (20\,{\rm deg},\ -10\,{\rm deg})$
motion 3	$(\theta_1^{\rm d}, \theta_2^{\rm d}) = (-2\,{\rm deg},\ 13\,{\rm deg})$
motion 4	$(\theta_1^{\rm d}, \theta_2^{\rm d}) = (-10\,{\rm deg},\ 20\,{\rm deg})$
motion 5	$(\theta_1^{\rm d}, \theta_2^{\rm d}) = (-7\,{\rm deg},\ 17\,{\rm deg})$
motion 6	$(\theta_1^{\rm d}, \theta_2^{\rm d}) = (17\,{\rm deg},\ -7\,{\rm deg})$
motion 7	$(\theta_1^{\rm d}, \theta_2^{\rm d}) = (-15\,{\rm deg},\ 25\,{\rm deg})$
motion 8	$(\theta_1^{\rm d}, \theta_2^{\rm d}) = (5\,{\rm deg},\ 5\,{\rm deg})$

why the paths were the same.

Figure 12 shows a simulation of rotation of a pinched object by an external force. As shown in Figure 12-(a), the pinched object rotates counterclockwise when the force is applied, though angle 0 of the two joints are fixed. As shown in Figure 12-(b) through (d), when the force is relaxed, the object rotates back to its initial orientation. Figure 13 shows the angle after the force has been relaxed. The simulation results agreed well with the observations shown in Figure 4.

Let us guide joint angles θ_1 and θ_2 to their desired values $\theta_1^{\rm d}$ and $\theta_2^{\rm d}$. The input torques on the joints of the right and left fingers are u_1 and u_2, respectively. Now, let us apply the following simple PID control laws to guide the joint angles to their desired values:

$$\begin{aligned} u_1 &= -K_{\rm P}(\theta_1 - \theta_1^{\rm d}) - K_{\rm D}\dot{\theta}_1 \\ &\quad -K_{\rm I}\int_0^t \{\theta_1(\tau) - \theta_1^{\rm d}\}\,{\rm d}\tau, \\ u_2 &= -K_{\rm P}(\theta_2 - \theta_2^{\rm d}) - K_{\rm D}\dot{\theta}_2 \\ &\quad -K_{\rm I}\int_0^t \{\theta_2(\tau) - \theta_2^{\rm d}\}\,{\rm d}\tau, \end{aligned}$$

where $K_{\rm P}$, $K_{\rm D}$, and $K_{\rm I}$ denote proportional, differential, and integral gains, respectively. Let us apply the sequence of desired values in Table II. Figure 14 shows the simulation results. We determined $K_{\rm P} = 300\,{\rm Nm/rad}$, $K_{\rm D} = 14\,{\rm Nm/(rad/s)}$, and $K_{\rm I} = 0.1\,{\rm Nm/(rad{\cdot}s)}$. In Figure 14-(a) and (b), respectively, the joint angles θ_1 and θ_2 of the right and left fingers converge to their desired values within one second. Figure 14-(c) and (d) show the object's position, and Figure 14-(e) shows its orientation. These figures show that the object is stable once the joint angles have stabilized, which suggests that the motion of the object is inherently stable without any external sensor feedback.

From the above simulations, we conclude that our proposed parallel distributed model provides a good explanation of grasping and manipulation by soft hemispherical fingertips. Moreover, soft hemispherical fingertips enable us to simplify the control law in grasping and manipulation.

VII. DISCUSSION

On observations and simulations prove that a pair of 1-DOF fingers with soft fingertips can regulate both grasping force and object orientation. The number of DOFs needed to grasp is summarized in Table III. It has been reported

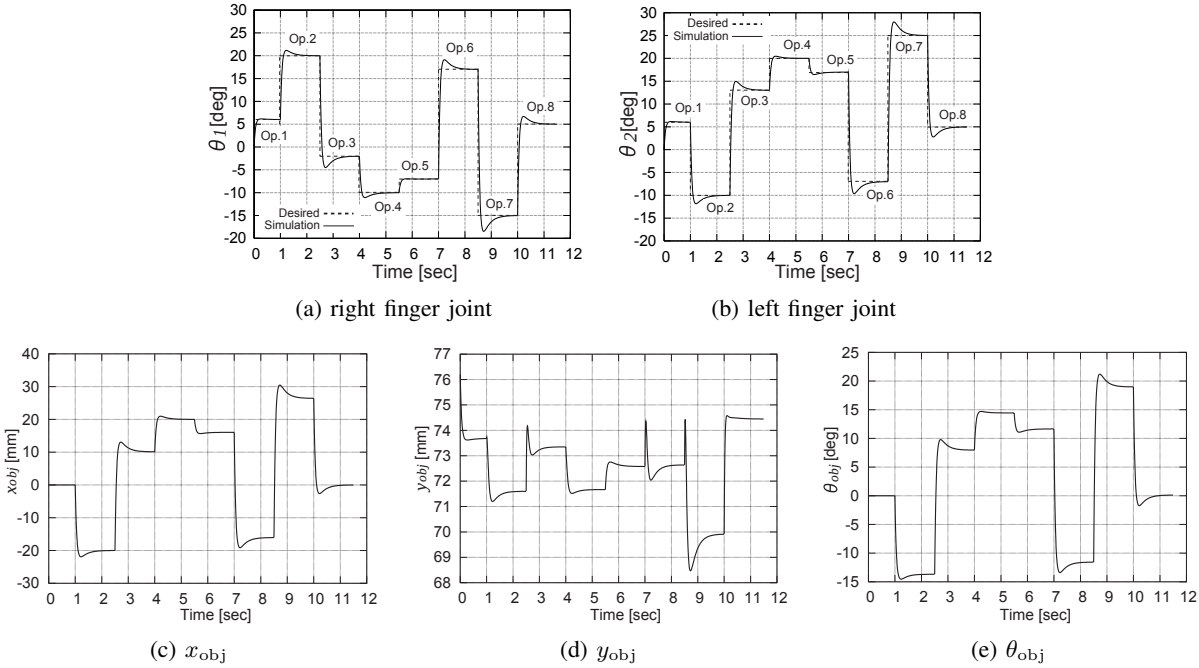

(a) right finger joint (b) left finger joint

(c) x_{obj} (d) y_{obj} (e) θ_{obj}

Fig. 14. Open loop control of object orientation

TABLE III
THE NUMBER OF DOFS NEEDED

	soft-fingered manipulation	hard-fingered manipulation
grasping	1	2
grasping and orientation	2	3

model	parallel	radial

that, based on a radially distributed model, for a pair of fingers with rigid fingertips to control the orientation of a rigid object, they would need at least 3 degrees of freedom, otherwise, regardless of their relative orientation, the moments on the object would not be balanced, and that the orientation of the object must be under sensor feedback. However, our study shows that the moments are actually balanced inherently by a pair of soft fingertips with one less degree of freedom, and that the orientation of the object can be controlled without sensor feedback. Consequently, the control law for the pair of 1-DOF soft fingertips is simpler.

Note that, in the parallel distributed model, the elastic potential energy of a soft fingertip depends on its angle relative to the grasped object. This dependency is due to fingertip being hemispherical with a hard back plate; the dependency does not exist for spherical fingertips because its shapes does not vary when they are rotated. In contrast, the hard plate behind the hemispherical soft fingertips imposes a boundary condition on their deformation, and results in their elastic energy varying with the relative orientation. Consequently, the structure of a finger consisting of a soft fingertip and a hard fingernail enhances dexterity in grasping and manipulation.

VIII. CONCLUSION AND RESEARCH PERSPECTIVE

We modeled a pair of hemispherical soft fingertips with 1-DOF grasping and manipulating a rigid object. First, we observed a pair of 1-DOF fingers with hemispherical soft fingertips pinching a rigid object. We found that they could grasp the object and control its orientation, in contrast to a previously reported theory based on a radially distributed model. Second, we proposed a parallel distributed model of the hemispherical soft fingertips, which are similar in structure to human fingertips in that they have a hard back plate that buttresses the soft pad, as do our fingernails. Third, we presented experimental results that support our parallel distributed model. Then, we formulated the dynamics of grasping and manipulation performed by the pair of 1-DOF fingers with soft fingertips. We showed that the dynamics can be described by Lagrange equations of motion with holonomic and nonhohonomic constraints due to the contact between each fingertip and the object. Finally, using our parallel distributed model, we simulated the soft fingertips grasping and manipulating the object and showed that our model agrees well with the observations.

In future studies, we will analyze the stability of the grasping and manipulation and will apply our model to grasping and manipulation by a multi-DOF, multi-fingered hand to investigate more comprehensively how the back plate/fingernail contributes to dexterity. Our model is planar, so we will extend it to a 3D model.

ACKNOWLEDGEMENT

This research was supported in part by the Ritsumeikan University 21st Century COE program “Micro Nanoscience Integrated Systems”.

REFERENCES

[1] Xydas, N. and Kao, I., *Modeling of Contact Mechanics and Friction Limit Surfaces for Soft Fingers in Robotics with Experimental Results*, Int. J. of Robotics Research, Vol. 18, No. 8, pp.941–950, 1999.

[2] Xydas, N., Bhagavat, M., and Kao, I., *Study of Soft-Finger Contact Mechanics Using Finite Elements Analysis and Experiments*, Proc. IEEE Int. Conf. on Robotics and Automation, pp.2179–2184, 2000.

[3] Kao, I. and Yang, F., *Stiffness and Contact Mechanics for Soft Fingers in Grasping and Manipulation*, IEEE Trans. on Robotics and Automation, Vol. 20, No. 1, pp.132–135, 2004.

[4] Johnson, K. L., *Contact Mechanics*, Cambridge University Press, 1985.

[5] Arimoto, S., Tahara, K., Yamaguchi, M, Nguyen, P, and Han, H. Y., *Principle of Superposition for Controlling Pinch Motions by means of Robot Fingers with Soft Tips*, Robotica, Vol. 19, pp.21–28, 2001.

[6] Nguyen, P. and Arimoto, S, *Performance of Pinching Motions of Two Multi-DOF Robotic Fingers with Soft-Tips*, Proc. IEEE Int. Conf. on Robotics and Automation, pp.2344–2349, 2001.

[7] Doulgeri, Z., Fasoulas, J., and Arimoto, S., *Feedback Control for Object Manipulation by a pair of Soft Tip Fingers*, Robotica, Vol. 20, pp.1–11, 2002.

[8] Fasoulas, J. and Doulgeri, Z., *Equilibrium Conditions of a Rigid Object Grasped by Elastic Rolling Contacts*, Proc. IEEE Int. Conf. on Robotics and Automation, pp.789–794, 2004.

[9] Takahiro Inoue and Shinichi Hirai, *Elastic Model of Deformable Fingertip for Soft-fingered Manipulation*, IEEE Trans. on Robotics, Vol. 22, No. 6, pp.1273–1279, 2006.

[10] Baumgarte, J., *Stabilization of Constraints and Integrals of Motion in Dynamical Systems*, Computer Methods in Applied Mechanics and Engineering, Vol. 1, pp.1–16, 1972.